LABORATORY SIMULATIONS OF SELF-POTENTIAL SIGNALS TO ASSIST GROUNDWATER STUDIES

Carlos Alberto Mendonça [ID][1], Suzan Sousa de Vasconcelos [ID][2], and
André Campos Guaragna Kowalski [ID][1]

[1]Universidade de São Paulo - USP, Instituto de Astronomia, Geofísica e Ciências Atmosféricas - IAG, São Paulo, SP, Brazil
[2]Universidade Federal da Bahia - UFBA, Instituto de Geociências, Departamento de Geofísica, Salvador, BA, Brazil

*Corresponding author email: carlos.mendonca@iag.usp.br

ABSTRACT. We present a brief history of experimental simulations with electrokinetic potential signals observed when common porous geological media are subjected to water flow regimes. The laboratory simulations at Instituto de Astronomia, Geofísica e Ciências Atmosféricas (IAG) of the Universidade de São Paulo (USP) had to overcome several challenges over years of research work, by developing experimental design, choice of materials, and software development to guide real data interpretation and definition of acquisition procedures to be implemented in practice. In this commemorative issue honouring the IAG/USP graduate program, we discuss some of our former results, including a set of original data for two laboratory experiments developed. The first experiment characterizes electrokinetic signals under controlled pumping regimes to illustrate the sensitivity of such potentials to structures with contrasting properties. The second study discusses model response for discrete fractures to guide field data interpretation to determine the hydraulic head in unconnected fractured systems by monitoring the variation of the electrokinetic potential after a borehole is pumped. In both cases, the experimental simulations are useful to understand the electric potentials of electrokinetic origin, pointing out their advantages in characterizing the subsurface hydraulic conditions when a borehole is pumped.

Keywords: electrokinetic potential; laboratory simulation; hydrogeophysics; crystalline aquifers; groundwater flow.

INTRODUCTION

Laboratory experimentation of geophysical methods in groundwater studies has been useful to validate model representations and interpret measurable quantities observed in field conditions. This kind of validation is particularly necessary when interpreting SP (self-potential) signals observed in many exploratory and site characterization scenarios with ground and borehole surveys. A core point motivating the application of SP data derives from the fact that such naturally occurring electrical potentials are indicative of active (not in equilibrium) processes forcing electrical charge transference in response to primary coupled fluxes of mass, charge or thermal energy (Onsager, 1931; Ishido and Pritchett, 1999). Despite easily being measured in field conditions, the interpretation of SP data based on coupled flux the-

ory requires substantial model approximations, not usually convincing that core elements in the underlying theory were kept into account by the interpreting models. In some cases, it is mandatory to check if predictions from coupled flux theory can indeed be verified in practical conditions, regarding common noise levels of field surveys or signal-enhancing capacity (pumping tests, for example) to produce measurable quantities. Experimental studies are then particularly important to suit interpreters with confidence about model representations and what should be expected in equivalent real conditions. The experimental approach developed at Instituto de Astronomia, Geofísica e Ciências Atmosféricas (IAG) of the Universidade de São Paulo (USP) over the last 15 years proved to be very effective in simulating scenarios representative of real-world problems when evaluating

groundwater systems and their dependence on aquifer properties. The present contribution puts in perspective two studies with SP signals from electrokinetic origin by discussing results from previously published works but extending their results with unpublished data supporting the mentioned works. Modelling of SP signals from redox procedures, another research line embraced with experimentation (Mendonça, 2008; Fachin et al., 2012), also achieved relevant milestones, for example in developing the concept of "biogeobattery" to explain natural attenuation processes in contaminated sites (Revil et al., 2010) and biogeochemical processes involving the organic matter mineralization in anoxic environments (Christensen et al., 2000). The present contribution, however, does not explore laboratory experiments with geobattery systems, a topic to be addressed with new data compilations. We briefly review basic aspects of coupled flux theory and the origin of SP fields from electrokinetic processes, a core phenomenon motivating the application of SP signals in hydrogeological studies.

THEORETICAL ASPECTS

The coupled flux theory was developed by Onsager (1931) and pioneered for geophysical problems by Marshall and Madden (1959). According to this theory, the spontaneous potential is the electric potential that arises coupled to a flux of water, heat or charge (in the case of redox processes) which is regarded as a kind of primary (or driving) flux. The primary flux is established in response to potential gradients of pressure, temperature, and redox conditions. For electrokinetic processes, let us consider a coupled system involving the primary flux of water, J_s, in a porous medium and its associated charge transport, J_q, for dissolved ions. The primary flux is driven by gradients in the pressure field, P, with a secondary electric potential, Φ in response such that

$$\begin{bmatrix} J_s \\ J_q \end{bmatrix} = - \begin{bmatrix} L_{11} & L_{12} \\ L_{21} & L_{22} \end{bmatrix} \cdot \begin{bmatrix} \nabla P \\ \nabla \Phi \end{bmatrix}, \quad (1)$$

the coupling parameters satisfying the Onsager reciprocity condition $L_{12} = L_{21} \equiv L$. For a laminar flow in saturated media, the parameter L_{11} satisfies

$$L_{11} = \frac{k}{\mu} \quad (2)$$

where k is the medium hydraulic permeability (m^2), and μ the water viscosity ($Pa\,s$). In Equation 1, $L_{22} = \sigma$ where σ is the electrical conductivity ($S\,m^{-1}$) of the percolating fluid. The cross-coupling parameter in Equation 1 is

$$L = \frac{kQ_v}{\mu}, \quad (3)$$

where Q_v is the volumetric charge density ($C\,m^{-3}$) of charge excess developed at the mineral/pore water interface. The flux of mass (water in this case) is then

$$J_s = -\frac{k}{\mu}\nabla P - \frac{kQ_v}{\mu}\nabla \Phi \quad (4)$$

and the coupled current flow

$$J_q = -\sigma\nabla\Phi - \frac{kQ_v}{\mu}\nabla P. \quad (5)$$

The first term of J_s in Equation 4 is the water percolation rate, v ($m\,s^{-1}$), satisfying Darcy equation

$$v = -\frac{k}{\mu}\nabla P. \quad (6)$$

Equation 4 can be approximated to $J_s \cong k/\mu\nabla P$ regarding typical values for the second coupled parameter, about two orders of magnitude lower than the first one (Nourbehecht, 1963). In the quasi-static regime, the electric potential Φ satisfies the null divergence condition, $\nabla J_q = 0$, thus featuring the secondary potential Φ as resulting from a current density J_p

$$\nabla(\sigma\nabla\Phi) = -J_p \quad (7)$$

with coupled current density

$$J_p = -\nabla(Q_v\Gamma_p) \quad (8)$$

where $\Gamma_p = -k/\mu\nabla P$ is the associated primary flow. Equivalent current sources, I_p, generating the potential Φ are situated at points where flux $Q_v\Gamma_p$ assumes non-null divergence, which stands for in-and-out points of water in a porous medium as well as interfaces with contrasting Q_v and k properties as illustrated in Figure 1. The volumetric charge density, Q_v, in Equation 4, is the macroscopic expression of an interface phenomenon called Electrical Double Layer (EDL) developed at the interface between the mineral grain and the pore water. Simple EDL formulations not accounting for ionic sorption have been used (Masliyah and Bhattacharjee, 2006), and more complex models incorporating mineral type and internal structures (Revil et al., 2012) further developed to characterize geological porous media. The structuring of charges at the mineral-solution interface (considering groundwater as an aqueous solution with dissolved salts) results from unbalanced charge distributions from electronegative oxygen sites in the crystal array of Si and Al oxides. The interface of common rock-forming minerals (quartz, feldspar, for example) thus shows a negative charge exposure which in contact with the pore solution creates a diffuse layer of positive charges (counter ions). The charge excess in the diffuse layer can move beyond a characteristic ("slipping plane") distance as the pore water flows while keeping an internal layer with fixed charges. Figure 2 illustrates the EDL charge distribution for a model with fixed and diffuse layers, accounting for

representations at the atomic scale for site occupation and characteristic lengths for molecules (water) and hydrated ionic species. The EDL thickness assuming the Gouy-Chapman model (Masliyah and Bhattacharjee, 2006), can be estimated as a function of the Debye length

$$k^{-1} = \left(\frac{\epsilon k_B T}{2e^2 z^2 n_\infty} \right)^{1/2}, \tag{9}$$

where ϵ is the dielectric permittivity of water ($\mathrm{F\,m^{-1}}$), T the temperature (K), z the valence of the ionic species, n_∞ the ionic volumetric concentration ($\mathrm{mol\,L^{-1}}$), $k_B = 1.3806503 \times 10^{-23}$ ($\mathrm{J\,K^{-1}}$) the Boltzmann constant, $e = 1.60217653 \times 10^{-19}$ (C) the unit charge of the electron. The amount of charge in the diffuse layer is given by Masliyah and Bhattacharjee (2006)

$$Q_v = \epsilon k \zeta \tag{10}$$

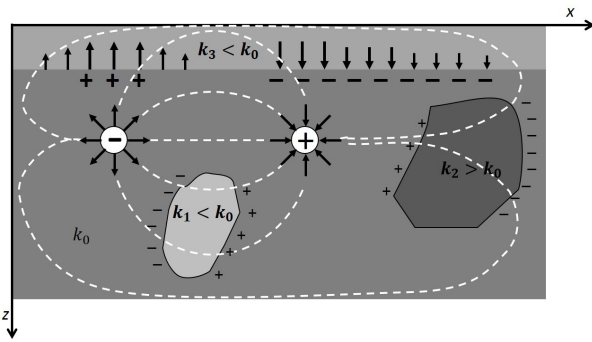which considers the zeta potential ζ to be the electric potential at the slipping plane.

Figure 1: Schematic representation of forced flow (arrows and dashed white lines) in a medium with contrasting properties, by using a pair of holes for water injection (left side) with extraction at the same rate (right side) and corresponding current negative-and-positive current terms at the pumping points and interfaces with contrasting properties. Comparison of electrokinetic with electric potentials from external sources serves as the basis for detecting the contrasting structures.

ELECTROKINETIC COUPLING PARAMETER

The electrokinetic coupling parameter, C ($\mathrm{mV\,Pa}$), is obtained as

$$C = -\frac{\epsilon \zeta}{\mu} \frac{\bar{\rho} g}{\sigma_f (1 + 2\mathrm{Du})} \tag{11}$$

where ϵ, μ and σ_f, $\bar{\rho}$ respectively, are the electric permittivity ($\mathrm{F\,m^{-1}}$), viscosity ($\mathrm{Pa\,s}$), electrical conductivity ($\mathrm{S\,m^{-1}}$), and volumetric density ($\mathrm{kg\,m^{-3}}$) for the pore fluid; for gravity attraction g ($\mathrm{m\,s^{-2}}$). The Dukhin number, Du, expresses the ratio between the

surface (dependent on the EDL charge excess) and volume (dependent on the pore fluid concentration) electrical conductivity values (Boleve et al., 2007).
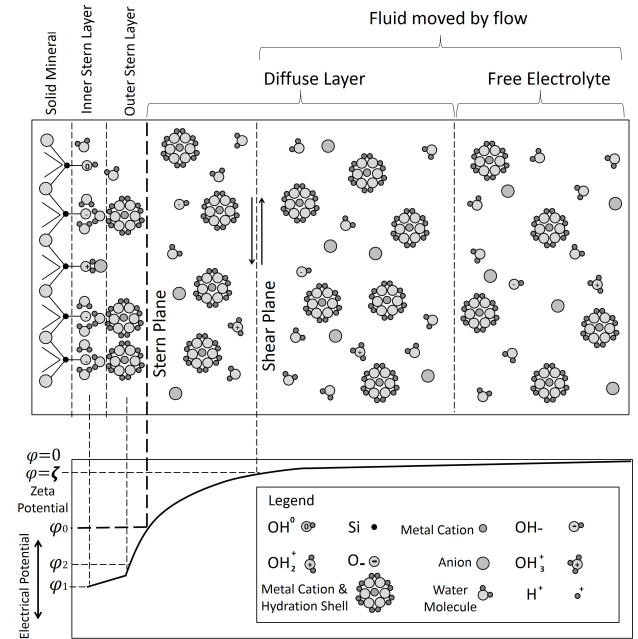

Figure 2: Schematic representation of the electrical double layer with fixed and diffuse layers for selective site occupation at the mineral phase, a slipping plane separating the fixed and the diffuse layers.

The measuring scheme in Figure 3a allows the determination of the electrokinetic coupling parameter by measuring the electric potential in response to variable water head differences applied to a porous medium sample (Mendonça, 2008). The schematic figure of the experimental apparatus shows a water keg connected by silicone hoses to the sample holder, which forces the water flow through the sample as the keg is raised to variable heights, $\Delta H = [50; 40; 30; 20; 10]$ cm, with resting stages ($\Delta H = 0$) at the beginning of each measurement sequence. Potential electrodes (Ag-AgCl) at the ends of the sample are connected to a high impedance voltmeter (U1252A-Agilent) to record the electric potential as a function of ΔH, for each stage recording (and then averaging) the potential for about 60 s. Repeated mean values for $\Delta H = 0$ are used to estimate instrumental drift. Figure 3b presents the electrical potential measured for $H = [0; 50; 40; 30; 20; 10; 0]$ cm, with well-defined flat response for each elevation. The coupling coefficient $C = \Delta\Phi/\Delta H$ in ($\mathrm{mV\,m^{-1}}$) (Ishido and Pritchett, 1999; Morgan et al., 1989) is determined as the slope of $\Delta\Phi$ versus ΔH curve, from which the electrokinetic coupling parameter in Equation 12 as

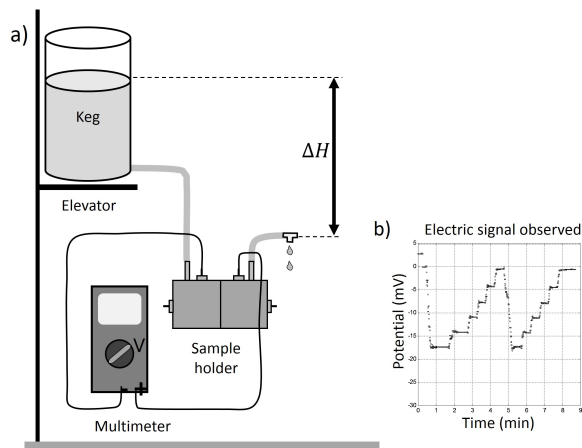$$L = -\frac{\sigma C}{\rho_w g}. \tag{12}$$

Figure 3: Schematics for measuring electrokinetic potentials as a function of hydraulic head differences; a) water head difference (ΔH) for a movable keg in an elevator with potential readings at the ends of an encapsulated porous medium with a high impedance voltmeter; b) typical electrokinetic response for variable $\Delta H = [0, 50, 40, 30, 20, 10, 0]$ cm in this case, for two repeated sequences. Each flat level in the recorded potential corresponds to a specific ΔH value. Mean values of potential values in the flat stages are plotted against the hydraulic head to determine the coupling parameter as the slope of the curve.

PUMPING TEST SIMULATIONS

The pumping test simulations were developed to verify if observed electrokinetic potentials can be modelled by current poles at water injection points and current distributions established by the primary flow at the interfaces with contrasting properties. Detailed model construction is described by Silva (2011) and procedures to obtain current source distributions from inverting the observed potentials discussed by Silva et al. (2021). As described by Vasconcelos et al. (2014), the testing tanks were mounted into transparent acrylic chambers, their top and bottom portions (4 cm) filled with water. Slabs of porous ceramic materials ($26 \times 10 \times 3$ cm) were sintered specifically for the experiments, with different mineral content (silica, alumina) with well-sieved grain sizes.

The experiment described by Vasconcelos et al. (2014) employed a porous ceramic sintered with #320 (mesh) grains of alumina (75% in volume) plus a mix of binder materials (25%) with vitrified enamel, feldspar, and kaolin. To simulate a discontinuity, the top of the slab was cut as illustrated in Figure 4. The tank in the second experiment had the same dimensions but the right 1/3 portion of the slab was sintered with #120 grains of alumina. This second model simulates a substrate with porosity contrast but with uniform mineral content. In both testing tanks, a set of 16 Ag-AgCl electrodes was installed at the upper chamber to record electrokinetic potentials

in response to selected pairs (AB, BC, and CD) subjected to dual pumping with a programmable syringe pump or electric potentials in response to external current sources at the same points. A dual syringe pump has a pair of equal-size syringes in opposite directions to simultaneously inject and extract a fixed quantity of water at a prescribed rate.
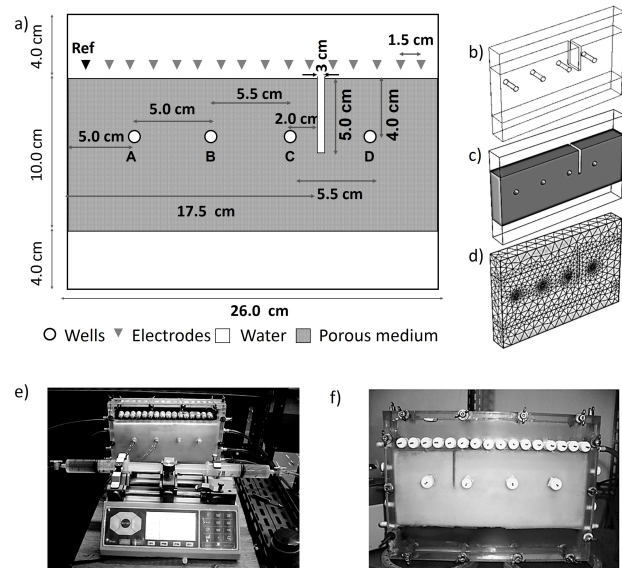

Figure 4: Experimental setup: a) tank layout with 16 potential electrodes in the upper water chamber; b) and c) geometrical representation of the model; d)mesh for finite-element modelling of coupled mass and current fluxes; e) tank front view with connections for pumping tests with a precise (programmable) dual syringe pump; f) opposite tank side view with electrodes for current injection (middle-depth) and potential readings (top). Holes A, B, C, and D were used to simulate boreholes with synchronous in-and-out pumping with programmable flow rates. A gap between holes C and D simulates a fracture at the top of a homogeneous medium. In the second testing tank (not in the figure) this 1/3 left portion of the medium is composed of coarser (#120) grains of alumina.

As shown in Figure 5, model responses from dual pumping and artificial current sources suggest a simple procedure to ascertain medium homogeneity near a pair of testing wells. As for pair AB, both fields can be modelled by a current bipole since this portion of the model is homogeneous, with minor deviations from the gap at the opposite side. This is not the case for testing points BC and DC closer to the gap, with substantial deviations in the electrokinetic response since the flow pattern is disturbed by the gap. Minor variations, however, affect the electric potential because model conductivity is not significantly modified by the insertion of a gap in the homogenous model.
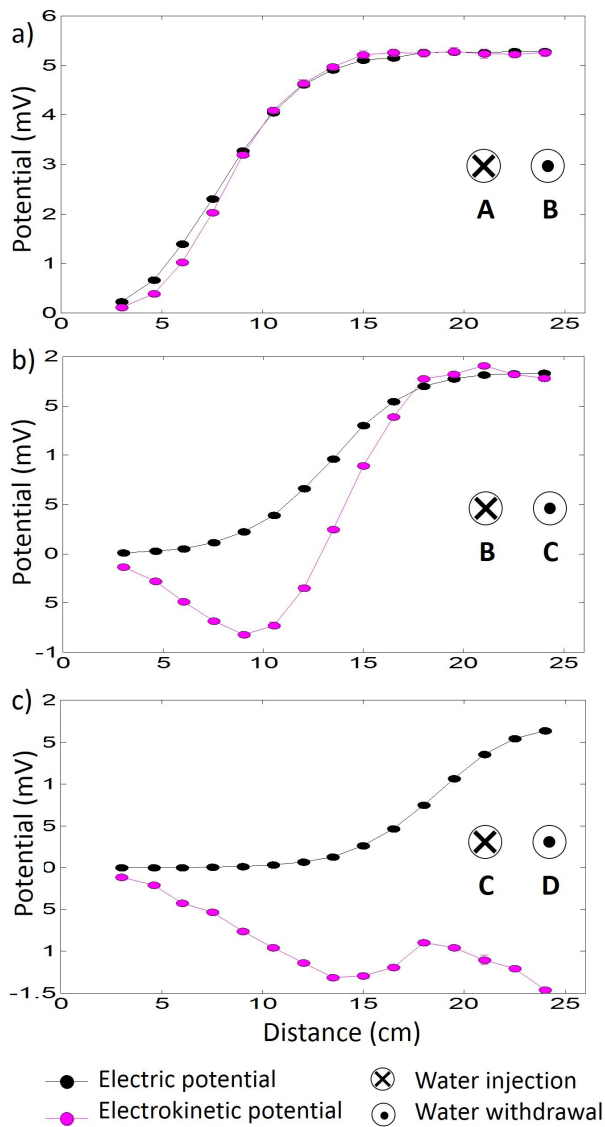
Figure 5: Experimental electric and electrokinetic measurements in a tank simulating a fracture: procedure made in the pairs (a) AB, (b) BC and (c) CD.

Figure 6: Electrokinetic simulation and calculated data: comparison at pairs (a) AB, (b) BC and (c) CD and (d) Cross-plot correlation.

To validate models with evaluated and observed potentials, simultaneous governing equations were solved numerically with finite-element models (Vasconcelos et al., 2014) with results as shown in Figure 6. This procedure required solutions of AC/DC electrical problems coupled with Darcy-Brinkman transport formulations, respectively for domains within the porous medium and water chambers. Modelling results confirm the correspondence in amplitude and polarity of potentials from pumping and artificial currents mainly at homogeneous portions of the model, but good agreement ($R^2 \approx 0.9$) in all testing pairs when comparing observed and evaluated electrokinetic signals. This result was a key point validating model representations with current distributions conditioned by model properties and their relationship with the primary flow pattern induced by a pumping procedure.
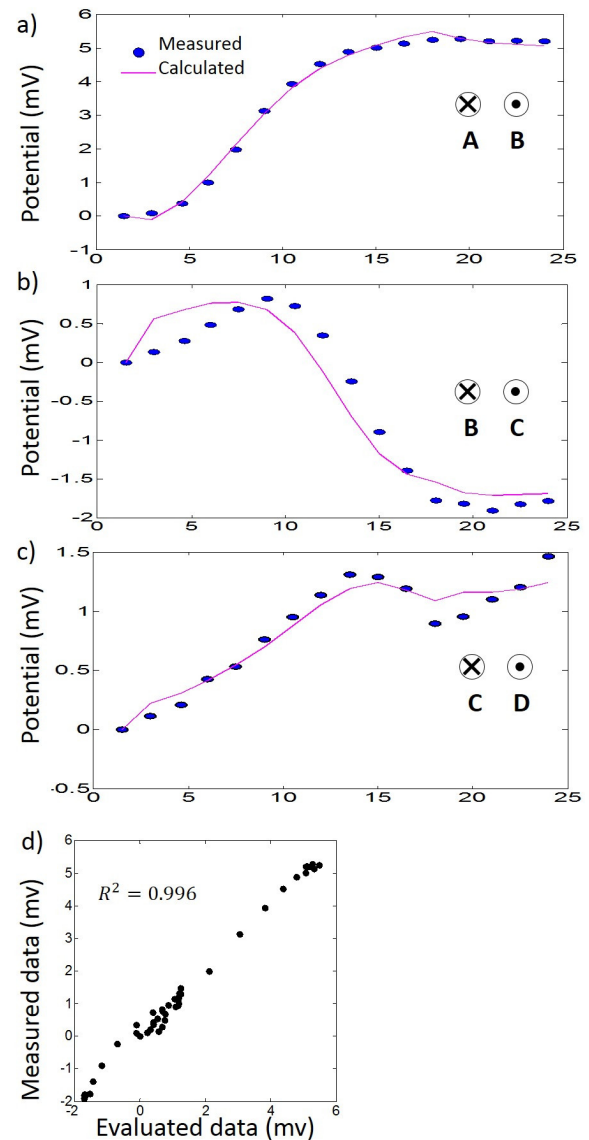
A second experimental tank simulated the contact of two media with uniform mineral content (alumina in both cases) but variable grain size. The 1/3 portion of the ceramic piece where the hole D was drilled had a coarser grain size (#120) and, as such, a higher porosity. The same tests with controlled water injection were applied as well as the procedure for current injection to evaluate the electric potential. Results in Figure 7 show the same equivalence pattern for testing holes at the homogeneous portion of the medium with deviations closer to the contrasting interface. However, if compared with results for the gap model (Figure 5), the contrasting porosity model shows minor deviations even closer to the interface (pair BC) but a substantial polarity change when the interface is in the middle position of the testing pair (CD). This kind of polarity inversion is expected for primary flows entering a coarser (more permeable) medium, as such

defining a characteristic pattern to infer the existence of more permeable domains in an aquifer or reservoir evaluation. The experiments in this line of research were repeated for two additional tanks, one preserving grain size but 1/3 portion sintered with silica, the other one with coarser silica. In all cases the model response patterns described by results in Figure 5 and Figure 7 were verified.
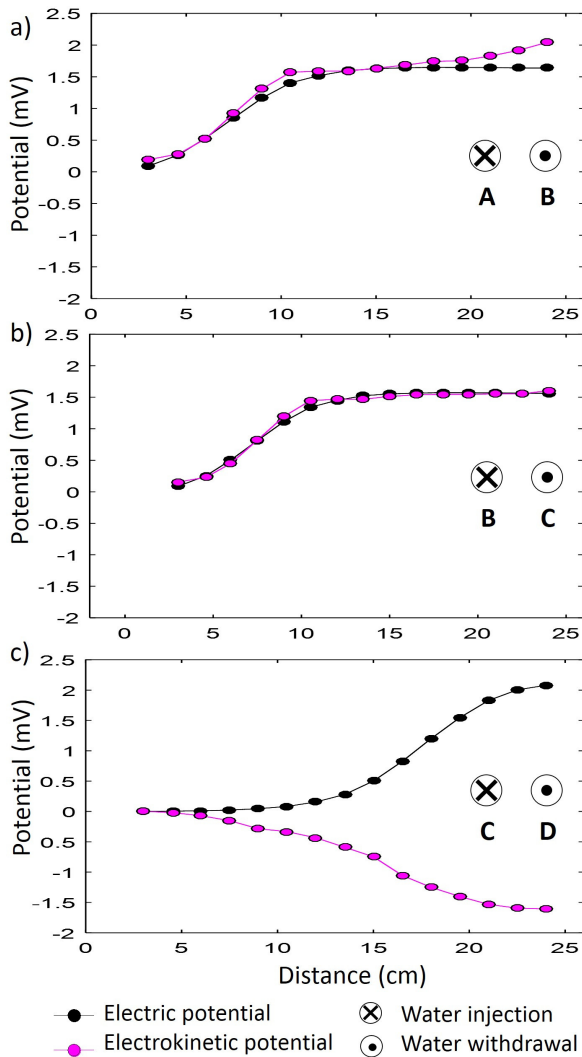

Figure 7: Experimental electric and electrokinetic measurements in the tank with porosity contrast, the homogeneous portion (#320) at holes ABC the interface with contrast (#120) in the middle of holes C and D. Results for pairs (a) AB, (b) BC and (c) CD, the injection point marked with 'x', the extraction point with '.'

HYDRAULIC HEAD DETERMINATION

Groundwater storage and transmissivity of aquifers in crystalline terrains are conditioned by connected fracture systems. Despite modern technology to visualize fractures and respective apertures from opti-

cal/acoustic imaging of the borehole wall, the identification of fractures effectively contributing to groundwater flow is still a challenging task of importance in hard rock tunnelling, subsurface mining or contaminant repository development. Kowalski et al. (2020) conceptualized a procedure to identify hydraulically active fractures by tracking their electrokinetic response after a well is pumped and left to recover to its previous condition. In this test, a transmissible fracture shows a characteristic sigmoidal variation in the electrokinetic potential, its polarity indicating flow direction (if entering or exiting the borehole), and its amplitude linearly varying as the static level is recovered. Since fractures with minor contributions to groundwater flow are not associated with SP variations, this simple recovery test may serve to identify fractures with transmissive properties. A characteristic water head assigning a null potential response (termed as zero-crossing potential) is of particular importance when determining the hydraulic head applied to a given fracture. More specifically, the zero-cross condition indicates that the water head in the borehole balances the water head a fracture is subjected to, indirectly inferring this relevant hydraulic parameter from a simple geophysical procedure.

The proposed recovering method was tested in field conditions (Kowalski et al., 2020) but some particularities of the test site (Kowalski et al., 2021), namely a single hydraulically active fracture at a very impermeable environment, left as open questions how the proposed test would respond if applied to boreholes with at least two fractured systems in more permeable environments. A laboratory-scale experiment was then outlined to simulate a situation in which a borehole intercepts two fractures, each one connected to aquifer systems with distinct hydraulic heads. This test sought to verify if the linearity between the electric potential and the applied hydraulic head is preserved for each electrokinetic system or disturbed by the short-circuited connection the borehole establishes.

The experimental setup as illustrated in Figure 8 was assembled, with two electrokinetic systems working as a couple of cells in parallel. Two different ceramic pieces were encapsulated in sealed chambers and then connected by silicone hoses to kegs with controlled heights. A keg installed in an elevator simulated the condition in which the water head in the borehole was lowered and then recovered step-by-step to its initial condition meanwhile recording the corresponding electric potential. The electrical potential was measured with a pair of Ag-AgCl electrodes located at both ends of the porous sample. The developed procedure starts by levelling the water head in the three kegs and recording instrumental drift (during 60 s) to be corrected. Next, one of the external kegs is elevated by 8.25 cm to simulate two electrokinetic systems subjected to distinct water heads. The keg in the elevator is then lowered (37.5 cm) and

raised at steps of 7.5 cm to simulate the recovery of the static level. For each step, the corresponding electric potential is recorded (60 s), averaged, and plotted as a function of the water head. The zero-crossing potentials for each cell are determined by least-squares fitting and compared with the known water heads initially applied to the cells (0.0 and 8.5 cm).
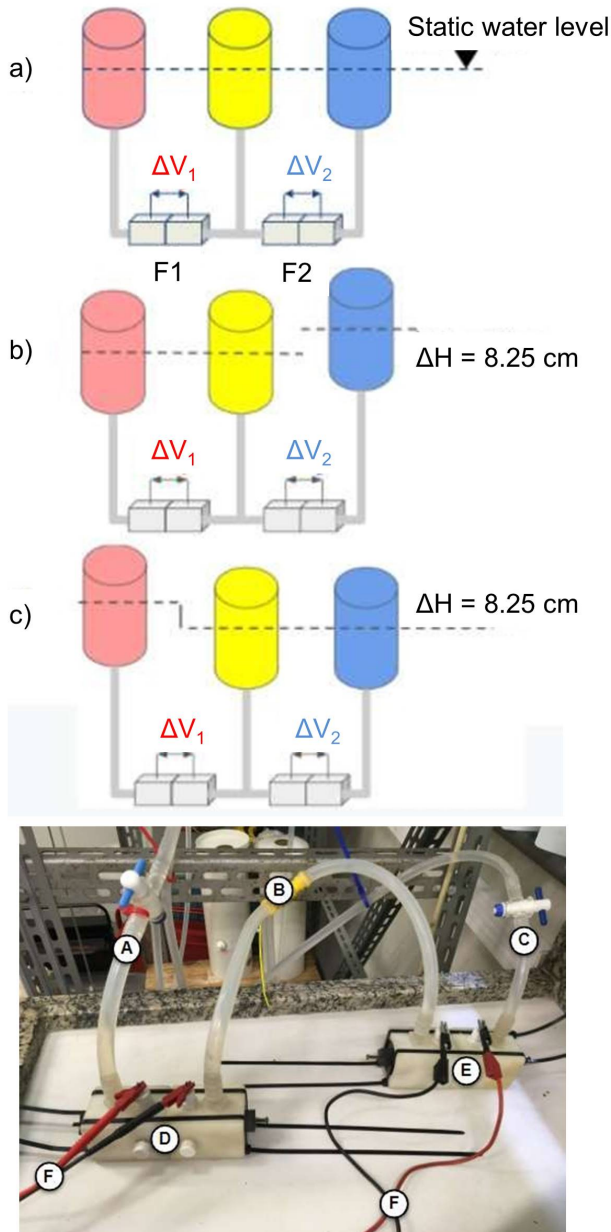
As shown in Figure 9, each cell has a different electrokinetic coupling parameter (5.7 ± 0.1 mV/m and 2.7 ± 0.1 mV/m), the same values determined in isolated tests with single chambers suggesting no distortions for a test with two cells in parallel. More importantly, the zero-crossing potential correctly identifies the hydraulic head for each cell within an acceptable error margin for the experiment; 7.8 ± 0.5 cm for the cell with 8.5 cm and -0.3 ± 0.5 cm for the cell levelled to the static level. Similar results (not shown in Figure 9) were obtained by changing the cell with an extra 8.5 cm hydraulic head, still accurately achieving hydraulic head and coupling parameter estimates.

Figure 8: Experimental arrangement used to simulate spontaneous potential measurements in a borehole intercepting two transmissive systems. Top: a), b) and c) stages of the experimental procedure consisting in initially levelling all kegs (coloured cylinders) and then applying an extra head (8.5 cm) to one of the cells while potential readings are simultaneously carried out (ΔV_1 and ΔV_2) for each cell. Bottom: picture of the sample holders and connections for data acquisition.
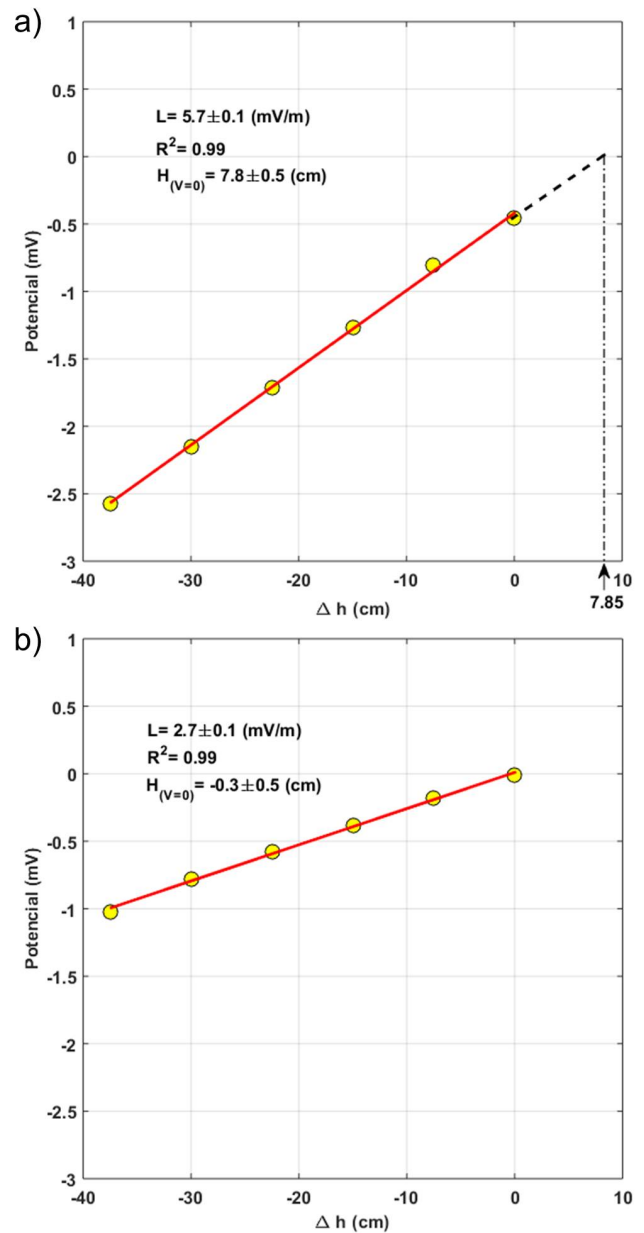

Figure 9: Recovery test with two parallel cells to determine their respective hydraulic heads using the zero-crossing criterion. Cell in a) with hydraulic head of 8.5 cm; cell in b) levelled to the static level simulating the borehole (0.0 cm).

PERSPECTIVES

Despite the simplicity of the models in common laboratory experiments, the results they provide usually are very effective in illustrating under what conditions a measurable electrokinetic signal can be expected when disturbing an aquifer system with dual pumping or monitoring its recovery to initial conditions after pumping. In the first case, the complexity of applying dual pumping to a pair of boreholes, no extension to a real application was developed. Nevertheless, much of what was learned with this experiment can be extended to real applications, for example by simplifying the pumping scheme with a single well while measuring SP signals at the ground surface or nearby wells. The second experiment illustrates a different situation in which a test of concept was implemented in a borehole but many questions were left unsolved about how a proposed testing procedure would respond in a more complex situation. Both cases illustrate the importance of laboratory investigations to assist real data interpretation to validate interpreting models to site characterization with the self-potential method. In practice, the study of a crystalline aquifer capacity exploitation depends on the characterization of fractured zones and their transmissivity for the allocation of groundwater collection wells. Understanding how the self-potential signal responds to the presence of discontinuities in the rocky environment, which can determine the flow of water, is crucial to determine the economic viability and the productivity in terms of volume and operating life wells.

ACKNOWLEDGMENTS

REFERENCES

Boleve, A., A. Crespy, A. Revil, F. Janod, and J.-L. Mattiuzzo, 2007, Streaming potentials of granular media: Influence of the Dukhin and Reynolds numbers: Journal of Geophysical Research: Solid Earth, **112**, B08204, doi: 10.1029/2006JB004673.

Christensen, T. H., P. L. Bjerg, S. A. Banwart, R. Jakobsen, G. Heron, and H. J. Albrechtsen, 2000, Characterization of redox conditions in groundwater contaminant plumes: Journal of Contaminant Hydrology, **45**, 165–241, doi: 10.1016/S0169-7722(00)00109-1.

Fachin, S. J., E. L. Abreu, C. A. Mendonça, A. Revil, G. C. Novaes, and S. S. Vasconcelos, 2012, Self-potential signals from an analog biogeobattery model: Geophysics, **77**, EN29–EN37, doi: 10.1190/geo2011-0352.1.

Ishido, T., and J. W. Pritchett, 1999, Numerical simulation of electrokinetic potentials associated with subsurface fluid flow: Journal of Geophysical Research: Solid Earth, **104**, 15247–15259, doi: 10.1029/1999JB900093.

Kowalski, A. C., C. A. Mendonça, and U. S. Ofterdinger, 2020, Fracture flow characterization with low-noise spontaneous potential logging: Groundwater, **59**, 16–23, doi: 10.1111/gwat.13009.

Kowalski, A. C., C. A. Mendonça, U. S. Ofterdinger, and H. R. Rocha, 2021, Fracture critical length estimative using percolation theory and well logging data: Journal of Environmental and Engineering Geophysics, **26**, 279–286, doi: 10.32389/JEEG21-019.

Marshall, D. J., and T. R. Madden, 1959, Induced polarization, a study of its causes: Geophysics, **24**, 790–816, doi: 10.1190/1.1438659.

Masliyah, J., and S. Bhattacharjee, 2006, Electrokinetic and colloidal transport phenomena: Wiley-Interscience: Hoboken, New Jersey. 707 pp.

Mendonça, C. A., 2008, Forward and inverse self-potential modeling in mineral exploration: Geophysics, **73**, F33–F43, doi: 10.1190/1.2821191.

Morgan, F., E. Williams, and T. Madden, 1989, Streaming potential properties of westerly granite with applications: Journal of Geophysical Research: Solid Earth, **94**, 12449–12461, doi: 10.1029/JB094iB09p12449.

Nourbehecht, B., 1963, Irreversible thermodynamic effects in inhomogeneous media and their applications in certain geoelectric problems: PhD thesis, Massachusetts Institute of Technology, Colorado School of Mine. Cambridge, Massachusetts. 121 pp.

Onsager, L., 1931, Reciprocal relations in irreversible processes. I.: Physical Review, **37**, 405, doi: 10.1103/PhysRev.37.405.

Revil, A., M. Karaoulis, T. Johnson, and A. Kemma, 2012, Review: Some low-frequency electrical methods for subsurface characterization and monitoring in hydrogeology: Hydrogeology Journal, **20**, 617–658, doi: 10.1007/s10040-011-0819-x.

Revil, A., C. A. Mendonça, E. A. Atekwana, B. Kulessa, S. S. Hubbard, and K. J. Bohlen, 2010, Understanding biogeobatteries: Where geophysics meets microbiology: Journal of Geophysical Research, **115**, G00G02, doi: 10.1029/2009JG001065.

Silva, N., 2011, Estudo de sinal elétrico de potencial espontâneo associado ao fluxo de água em meios porosos: PhD thesis, Universidade de São Paulo, São Paulo, SP, Brazil. 98 pp.

Silva, N., S. S. de Vasconcelos, and C. A. Mendonça, 2021, Constraints for mapping subsurface current sources: Brazilian Journal of Geophysics, **39**, 479–488, doi: 10.22564/rbgf.v39i4.2099.

Vasconcelos, S. S., C. A. Mendonça, and N. Silva, 2014, Self-potential signals from pumping tests in laboratory experiments: Geophysics, **79**, EN125–EN133, doi: 10.1190/geo2013-0444.1.

Mendonça, C.A.: conceived the ideas and research hypotheses; academic guidance and management of researches at laboratory studies and modelling simulations. Thus, developed the line of experimental research in its institution from creation, implementation, description and production of the article; **Vasconcelos, S.S.:** worked on the experimental tank setup to understand the behavior of electrokinetic potential in continuos and uncontinuos medium during pumping tests. Performed measures, analyzed results and described the observations (as part of her doctoral thesis) producing the textual description of the methodology, results and figures; **Kowalski, A.C.G.:** worked on the experimental keggings setup to understand the correlation between transmissivity in fracturated cristalinne acquifer and electrokinetic potential signal. Performed measures, analyzed results and described the observations (as part of his doctoral thesis) producing the textual description of the methodology, results and figures.